High aspect ratio taper-free microchannel fabrication using femtosecond Bessel beams

M. K. Bhuyan[1], F. Courvoisier[1]*, P.-A. Lacourt[1], M. Jacquot[1], L. Furfaro[1], M. J. Withford[2] and J. M. Dudley[1]

[1]*FEMTO-ST Institute, Department of Optics P.M. Duffieux, UMR CNRS 6174, Université de Franche-Comté, 25030 Besançon, France*

[2]*CUDOS and MQ Photonics, Department of Physics, Macquarie University, New South Wales, 2109, Australia*

**francois.courvoisier@femto-st.fr*

Abstract: We present a systematic study of femtosecond laser microchannel machining in glass using nondiffracting Bessel beams. In particular, our results identify a source and focusing parameter working window where high aspect ratio taper-free microchannels can be reproducibly produced without sample translation. With appropriate source parameters, we machine channels of 2 µm diameter and with aspect ratios up to 40. We propose the filamentation stability of the Bessel beam propagation as the critical factor underlying the controlled and reproducible results that have been obtained.

©2010 Optical Society of America

OCIS codes: (190.7110) Ultrafast nonlinear optics; (320.2250) Femtosecond phenomena; (350.3390) Laser materials processing; (070.6120) Spatial light modulators; (160.2750) Glass and other amorphous materials

References and links

1. R. R. Gattass, and E. Mazur, "Femtosecond laser micromachining in transparent materials," Nat. Photonics **2**(4), 219–225 (2008).
2. G. Della Valle, R. Osellame, and P. Laporta, "Micromachining of photonic devices by femtosecond laser pulses," J. Opt. A, Pure Appl. Opt. **11**(1), 013001 (2009).
3. G. M. Whitesides, "The origins and the future of microfluidics," Nature **442**(7101), 368–373 (2006).
4. D. Psaltis, S. R. Quake, and C. Yang, "Developing optofluidic technology through the fusion of microfluidics and optics," Nature **442**(7101), 381–386 (2006).
5. H. Craighead, "Future lab-on-a-chip technologies for interrogating individual molecules," Nature **442**(7101), 387–393 (2006).
6. L. C. Campbell, M. J. Wilkinson, A. Manz, P. Camilleri, and C. J. Humphreys, "Electrophoretic manipulation of single DNA molecules in nanofabricated capillaries," Lab Chip **4**(3), 225–229 (2004).
7. H. Varel, D. Ashkenasi, A. Rosenfeld, M. Wahmer, and E. E. B. Campbell, "Micromachining of quartz with ultrashort laser pulses," Appl. Phys., A Mater. Sci. Process. **65**(4-5), 367–373 (1997).
8. J. Schwarz, and J. C. Diels, "UV filaments and their application for laser-induced lightning and high-aspect-ratio hole drilling," Appl. Phys., A Mater. Sci. Process. **77**, 185–191 (2003).
9. L. Luo, D. Wang, C. Li, H. Jiang, H. Yang, and Q. Gong, "Formation of diversiform microstructures in wide-bandgap materials by tight-focusing femtosecond laser pulses," J. Opt. A, Pure Appl. Opt. **4**(1), 105–110 (2002).
10. Y. Bellouard, A. Said, M. Dugan, and P. Bado, "Fabrication of high-aspect ratio, micro-fluidic channels and tunnels using femtosecond laser pulses and chemical etching," Opt. Express **12**(10), 2120–2129 (2004), http://www.opticsinfobase.org/oe/abstract.cfm?URI=oe-12-10-2120.
11. D. Wortmann, J. Gottmann, N. Brandt, and H. Horn-Solle, "Micro- and nanostructures inside sapphire by fs-laser irradiation and selective etching," Opt. Express **16**(3), 1517–1522 (2008), http://www.opticsinfobase.org/oe/abstract.cfm?URI=oe-16-3-1517.
12. S. Kiyama, S. Matsuo, S. Hashimoto, and Y. Morihira, "Examination of Etching Agent and Etching Mechanism on Femotosecond Laser Microfabrication of Channels Inside Vitreous Silica Substrates," J. Phys. Chem. C **113**(27), 11560–11566 (2009).
13. Y. Li, K. Itoh, W. Watanabe, K. Yamada, D. Kuroda, J. Nishii, and Y. Jiang, "Three-dimensional hole drilling of silica glass from the rear surface with femtosecond laser pulses," Opt. Lett. **26**(23), 1912–1914 (2001).
14. K. Ke, E. F. Hasselbrink, Jr., and A. J. Hunt, "Rapidly prototyped three-dimensional nanofluidic channel networks in glass substrates," Anal. Chem. **77**(16), 5083–5088 (2005).
15. L. Sudrie, A. Couairon, M. Franco, B. Lamouroux, B. Prade, S. Tzortzakis, and A. Mysyrowicz, "Femtosecond laser-induced damage and filamentary propagation in fused silica," Phys. Rev. Lett. **89**(18), 186601 (2002).
16. A. Couairon, and A. Mysyrowicz, "Femtosecond filamentation in transparent media," Phys. Rep. **441**(2-4), 47–189 (2007).

#119015 - $15.00 USD Received 23 Oct 2009; revised 30 Nov 2009; accepted 30 Nov 2009; published 4 Jan 2010

17. K. C. Vishnubhatla, N. Bellini, R. Ramponi, G. Cerullo, and R. Osellame, "Shape control of microchannels fabricated in fused silica by femtosecond laser irradiation and chemical etching," Opt. Express **17**(10), 8685–8695 (2009), http://www.opticsinfobase.org/oe/abstract.cfm?URI=oe-17-10-8685.
18. J. Durnin, J. J. Miceli, Jr., and J. H. Eberly, "Diffraction-free beams," Phys. Rev. Lett. **58**(15), 1499–1501 (1987).
19. Y. Matsuoka, Y. Kizuka, and T. Inoue, "The characteristics of laser micro drilling using a Bessel beam," Appl. Phys., A Mater. Sci. Process. **84**(4), 423–430 (2006).
20. F. Courvoisier, P.-A. Lacourt, M. Jacquot, M. K. Bhuyan, L. Furfaro, and J. M. Dudley, "Surface nanoprocessing with nondiffracting femtosecond Bessel beams," Opt. Lett. **34**(20), 3163–3165 (2009).
21. J. Amako, D. Sawaki, and E. Fujii, "Microstructuring transparent materials by use of nondiffracting ultrashort pulse beams generated by diffractive optics," J. Opt. Soc. Am. B **20**(12), 2562–2568 (2003).
22. V. Zambon, N. McCarthy, and M. Piché, "Fabrication of photonic devices directly written in glass using ultrafast Bessel beams," Proc. SPIE **7099**, 70992J/1–5 (2008).
23. D. J. Hwang, K. Hiromatsu, H. Hidai, and C. P. Grigoropoulos, "Self-guided glass drilling by femtosecond laser pulses," Appl. Phys., A Mater. Sci. Process. **94**(3), 555–558 (2009).
24. N. T. Nguyen, A. Saliminia, S. L. Chin, and R. Vallee, "Control of femtosecond laser written waveguides in silica glass," Appl. Phys. B **85**(1), 145–148 (2006).
25. R. An, Y. Li, Y. Dou, H. Yang, and Q. Gong, "Simultaneous multi-microhole drilling of soda-lime glass by water-assisted ablation with femtosecond laser pulses," Opt. Express **13**(6), 1855–1859 (2005), http://www.opticsinfobase.org/oe/abstract.cfm?URI=oe-13-6-1855.
26. P. Polesana, M. Franco, A. Couairon, D. Faccio, and P. Di Trapani, "Filamentation in Kerr media from pulsed Bessel beams," Phys. Rev. A **77**(4), 043814 (2008).
27. Z. Song, Z. Zhang, and T. Nakajima, "Transverse-mode dependence of femtosecond filamentation," Opt. Express **17**(15), 12217–12229 (2009), http://www.opticsinfobase.org/oe/abstract.cfm?URI=oe-17-15-12217.
28. D. J. Hwang, T. Y. Choi, and C. Grigoropoulos, "Liquid-assisted femtosecond laser drilling of straight and three dimensional microchannels in glass," Appl. Phys., A Mater. Sci. Process. **79**(3), 605–612 (2004).
29. D. Ashkenasi, M. Lorenz, R. Stoian, and A. Rosenfeld, "Surface damage threshold and structuring of dielectrics using femtosecond laser pulses: the role of incubation," Appl. Surf. Sci. **150**(1-4), 101–106 (1999).
30. A. Zoubir, L. Shah, K. Richardson, and M. Richardson, "Practical uses of femtosecond laser micro-materials processing," Appl. Phys., A Mater. Sci. Process. **77**, 311–315 (2003).
31. D. Rayner, A. Naumov, and P. Corkum, "Ultrashort pulse non-linear optical absorption in transparent media," Opt. Express **13**(9), 3208–3217 (2005), http://www.opticsinfobase.org/oe/abstract.cfm?URI=oe-13-9-3208.

1. Introduction

Femtosecond laser micromachining is a versatile materials processing technology suitable for fabricating a wide range of structures in transparent media [1,2]. It holds particular promise for microfluidics applications where high quality sub-10 μm channels are essential structures in the development of system-scale lab-on-chip and DNA analysis [3–6]. Femtosecond microchannel machining in various glasses has been the subject of many previous studies and, whilst debris redeposition and tapering effects precludes high aspect ratio microchannel fabrication using simple front-surface illumination in air, several more sophisticated approaches have been developed. These include micromachining in vacuum [7], micromachining with filamentary propagation [8,9], micromachining combined with selective etching [10–12], and micromachining the reverse side of the sample using water immersion for debris removal [13]. Although these approaches have yielded promising results [1,2,7,9,14], they nonetheless suffer from a variety of complexities and drawbacks: micromachining in vacuum removes the attractive reconfigurability of the femtosecond machining approach; filamentary propagation of Gaussian beams yields non-uniform structural damage [15] and multiple filamentation can appear at high pulse powers [16]; selective etching requires significant additional processing time and inverse-conical illumination for taper-free channels [14,17]; reverse-side machining needs precise adjustment of sample position and translation velocity to scan the ablation site through the sample.

These previous studies, however, have all used femtosecond lasers with transverse Gaussian beam intensity profiles. In this paper, however, we describe an alternative and original approach using high-aspect ratio Bessel beams [18] to overcome many of the difficulties associated with femtosecond micromachining with Gaussian beams. Although femtosecond Bessel beam machining has been investigated for laser processing in metals [19], laser surface nanoprocessing [20] and index modification in glass [21,22], to our knowledge, the results here are the first to describe its application to the fabrication of glass microchannels. Our results are obtained with input powers such that the structural

#119015 - $15.00 USD Received 23 Oct 2009; revised 30 Nov 2009; accepted 30 Nov 2009; published 4 Jan 2010
(C) 2010 OSA

modification arises from the filamentary propagation of the incident beam in the glass material, and we observe both regions of refractive index modification and ablation-induced channel formation or drilling [23,24]. In contrast to previous studies using Gaussian beams where micromachining in the filamentary regime may lead to the presence of significant taper and/or instabilities [23,25], our results show that Bessel beams can be used to generate high quality taper-free channels of around ~2 µm diameter and ~80 µm length in a straightforward setup without the need for any sample translation. We interpret these results in terms of a specific regime of stable filament formation [26,27], and identify a working window for the practical use of Bessel beams in glass micromachining applications.

2. Experimental setup

Our experimental setup is shown in Fig. 1. We generate a Bessel beam using a spatial light modulator (SLM) to imprint the spatial phase of an axicon onto the beam of a regeneratively amplified (Spectra Physics Spitfire) 100 fs Ti:Sapphire laser (Ti:Sa) operating at central wavelength 800 nm. For focusing onto a sample, the Bessel beam was de-magnified by a factor of 110 using a telescope consisting of a f = 1 m lens and a x20 microscope objective. The resulting Bessel beam has conical angle $\theta = 10°$, central spot diameter d = 1.5 µm FWHM and depth of focus D = 150 µm FWHM in air. The sample was placed in the Bessel beam focal region and imaged through the focusing objective using a CCD camera as shown in the figure. An additional CCD camera (not shown) and a x40 magnification imaging system was translated through the focal region without the sample present in order to characterize the intensity distribution of the Bessel beam as a function of longitudinal propagation distance. These measurements were made with 5 µm longitudinal resolution. Note that with our setup, the point of beam onset is the focal point of the microscope objective and the working distance is several mm; this is important for processing thick samples and/or high speed sample displacements. This also facilitates positioning the onset of the Bessel beam at different points in the sample as discussed below.

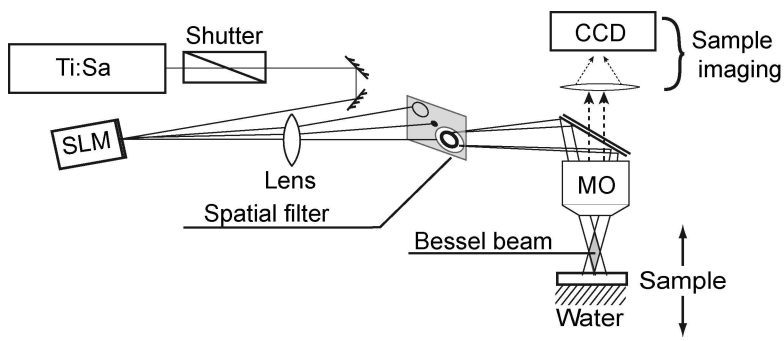

Fig. 1. Schematic of Bessel beam generation, sample positioning and imaging setups.

3. Influence of focusing geometry

For 150 µm thickness Corning 0211 borosilicate glass samples, we first present results comparing the quality of the machined structures obtained for different focussing geometries as shown in Fig. 2. This illustrative figure showing different geometries and sample positions nonetheless uses the experimentally-imaged longitudinal beam profile, corrected numerically for the effects of refraction in the sample. Note that a static Gaussian beam plotted in the same way as in the figure would appear as a single bright point at the waist with reduced intensity as the beam diverges. The illustrative results we discuss below using Bessel beams can be usefully compared with the many previous studies of Gaussian beam structuring with or without sample translation and water assistance; see for example Fig. 1 of [7], Fig. 3 of [23], Fig. 11 of [28].

#119015 - $15.00 USD Received 23 Oct 2009; revised 30 Nov 2009; accepted 30 Nov 2009; published 4 Jan 2010
(C) 2010 OSA

Since the glass thickness and the depth of focus in the sample were comparable, the top image in Fig. 2(a) shows what might be expected to be a focusing geometry that would yield good results. Here, the sample is centered longitudinally about the beam extension and surrounded by air. The top image in Fig. 2(b) shows the corresponding damage induced in the glass after illumination by 500 laser shots at a source repetition rate of 5 kHz with incident pulses of energy 7.7 µJ. Note that this image was obtained using Differential Interference Contrast (DIC) microscopy with 0.5 µm diffraction-limited resolution. It is clear that this geometry gives unsatisfactory results because the damage is inhomogeneous along the propagation direction. Note also that although we show results at only one set of source parameters, we confirmed through additional experiments that this geometry uniformly yielded inhomogeneous damage and poor quality channel structures.

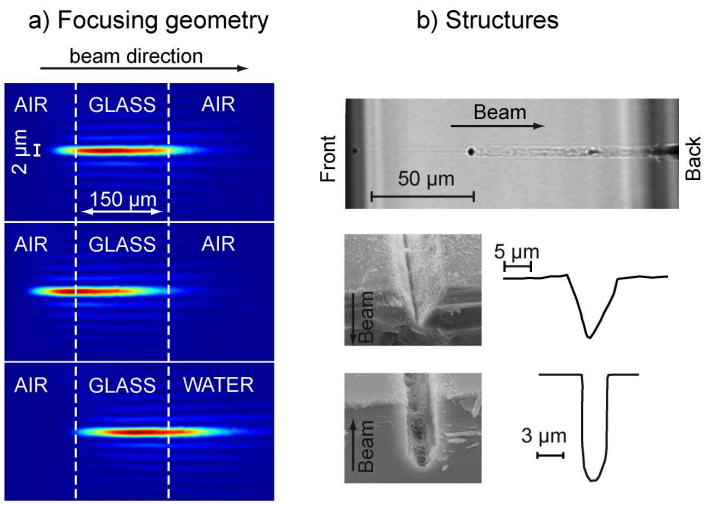

Fig. 2. (a) Different focusing geometries as shown, with superimposed measured intensity profile of the Bessel beam. (b) Structures obtained for each focusing geometry (see text). For the two microtrench SEM images, numerically-extracted line profiles are also shown. The scales shown apply to both horizontal and vertical directions and the profiles are corrected for tilt. Beam directions are shown in the figure.

In other experiments, we investigated both front-side and rear-side illumination of the sample with and without water immersion for debris evacuation. The center panel in Fig. 2(a) shows the geometry for front-side ablation in air and the bottom panel in Fig. 2(a) shows the geometry for rear-side ablation with rear-side water immersion. The front-side geometry in this case is, in fact, that which has been previously studied with Bessel beam ablation of metals, where it was found to lead to significant channel tapering [19]. In our experiments, we observed the same undesirable tapering behavior when machining in glass with this geometry. To illustrate this effect particularly clearly, we show in the figure results of additional experiments where we machined trenches rather than channels by translating the sample perpendicularly to the beam, as this provides a clearer view of the cross section of the machined features. The middle panel in Fig. 2(b) shows a Scanning Electron Microscope (SEM) image of a machined surface micro-trench using front-side illumination with 100 passes at 8 µJ /pulse an a repetition rate of 5 kHz, and a translation speed ~0.5 mm/s. We attribute the formation of the taper to the fact that accumulation of debris on the surface reduces the ablation threshold, allowing the wings (sidelobes) of the incident beam to contribute to material removal [29]. In contrast, the geometry using rear-side illumination with water to remove evacuated debris overcomes this problem. A microtrench machined using this approach (with parameters as above) is shown in the bottom image of Fig. 2(b) and the improved sidewall quality is immediately apparent. Note that the width of the trench (3 µm) is comparable to the diameter of the central lobe of the Bessel beam (1.5 µm FWHM, 3.5

#119015 - $15.00 USD Received 23 Oct 2009; revised 30 Nov 2009; accepted 30 Nov 2009; published 4 Jan 2010
(C) 2010 OSA

μm at $1/e^2$); we discuss this in more detail in Section 5. It is the use of this focusing geometry with Bessel beams without sample translation that also yields high-quality microchannel fabrication. This is the focusing geometry used in all the experiments reported below.

4. Experimental results

In this section, we present a series of results showing how the characteristics of microchannels machined using Bessel beams vary with input pulse parameters. The first results in Fig. 3 show measured DIC images of machined channel structures for two incident pulse energies of (a) 7 μJ and (b) 10.7 μJ at a repetition rate of 100 Hz. We can clearly identify regions of drilled channels (black regions) as well as refractive-index modification (light regions) [28], and the figure also allows us to identify and discuss several characteristic features of the channel formation process. In contrast to comparable studies carried out using Gaussian beams [23,30], the channels and structures in Fig. 3(a) and 3(b) are free of visible tapering over their length, and we stress again that these results are obtained without any sample translation.

For both pulse energies, in the regime where machining is carried out with less that 500 shots, the formation of channels appears stochastic from run-to-run; some series of shots induce refractive index changes, other series of shots induce channels. Nonetheless, for more than 500 shots, the channel properties (length and diameter) stabilize significantly. That is, all series of shots yield clear channel formation, although there is some residual run-to-run variation in the channel length. This near-constant length above 500 shots is shown in Fig. 3(a) for 7 μJ pulse energy. Error bars are calculated from measurements on 5 channels machined using identical parameters. We have not examined this transition from stochastic to deterministic drilling in detail, but we note that a similar "pulse number threshold" has been reported for self-guided Gaussian beam drilling, and attributed to a necessary incubation period for the creation of initial material defects and a sustained plasma channel [23].

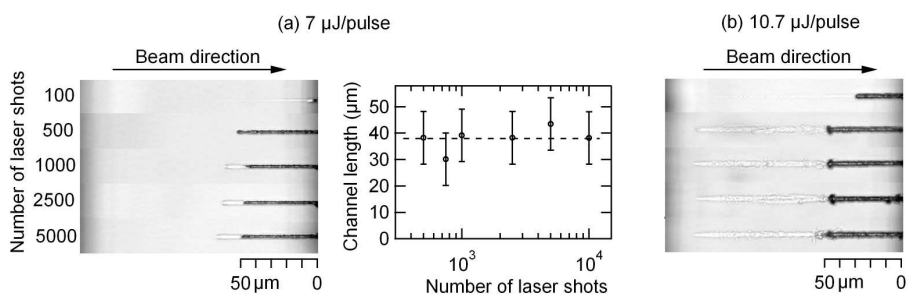

Fig. 3. Results illustrating channel formation and evolution of channel length with number of shots at 100Hz repetition rate. Differential Interference Contrast (DIC) images are shown for (a) 7 μJ/pulse and (b) 10.7 μJ/pulse. The dark regions (on the right hand side of each image) are the microchannels whereas the lighter regions of modified material represent index change only. The central panel shows dependence of length on number of shots for 7 μJ/pulse energy. The dashed lines show the mean of 39 μm calculated over range 500-10000 shots.

At a higher pulse energy as shown in Fig. 3(b), we see similar length stabilization at more than 500 shots, and we remark on three additional observations. Firstly, the channel diameter does increase slightly with pulse energy, but is independent of the number of shots used provided we are above the observed 500 shot stability threshold. Secondly, we can see from the DIC micrograph how the higher pulse energy leads to increased (and undesirable) longitudinal structure along the length of the channel. Finally, we note a bulb-like feature that is apparent between the refractive-index modified zone and the onset of the uniform-diameter channel. The complex nonlinear dynamics at this transition point make it difficult to unambiguously attribute this morphology to any one specific process, but we note that such a feature is consistent with a mechanism of nonlinear self-focusing induced shock wave generation [14].

#119015 - $15.00 USD Received 23 Oct 2009; revised 30 Nov 2009; accepted 30 Nov 2009; published 4 Jan 2010
(C) 2010 OSA

We examine the dependence of channel morphology on pulse energy in more detail below, but we briefly complete our discussion of channel length by showing in Fig. 4 the dependence of channel length on pulse repetition rate. These results were obtained with 7.6 μJ/pulse energy and 1000 laser shots. (In this context, we note that we found that the use of 1000 shots was a convenient experimental guideline to generate reproducible and non-stochastic structures over a wide range of input pulse parameters.)

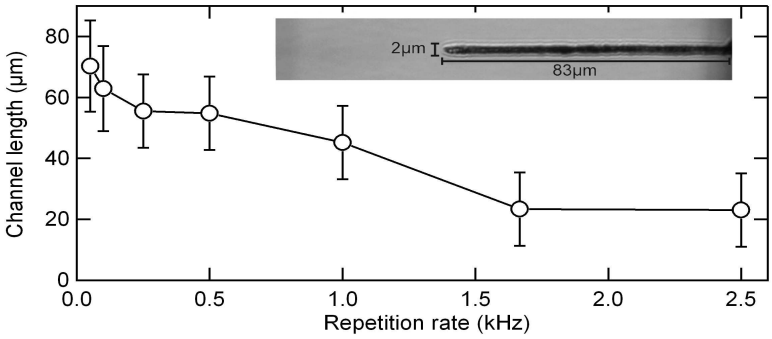

Fig. 4. Dependence of channel length on repetition rate for a 7.6 μJ/pulse and 1000 laser shots. A particularly high-quality result showing a 2 μm channel with aspect ratio of around 40 observed at 50 Hz is shown as the inset to this figure.

The channel length clearly decreases with increased repetition rates, consistent with previous experiments using Gaussian beam illumination [13,28]. It arises physically because an increased time between successive shots allows more efficient debris removal. Note that the channel diameter was constant at 2 ± 0.5 μm over the range of repetition rates plotted in the figure and aspect ratios as high as 40 were obtained at repetition rates of 50 Hz. A particularly high quality channel is shown in the inset.

The results showing our detailed study of channel morphology as a function of incident pulse energy are shown in Fig. 5. For a repetition rate of 100 Hz and using 1000 laser shots, we determined the mean channel length and diameter by using DIC microscopy to image a series of 10 channels which were machined at each value of pulse energy. The pulse energy was measured after the microscope objective so that it corresponds to that incident on the sample. Typical DIC images for each energy value are also shown.

#119015 - $15.00 USD Received 23 Oct 2009; revised 30 Nov 2009; accepted 30 Nov 2009; published 4 Jan 2010
(C) 2010 OSA

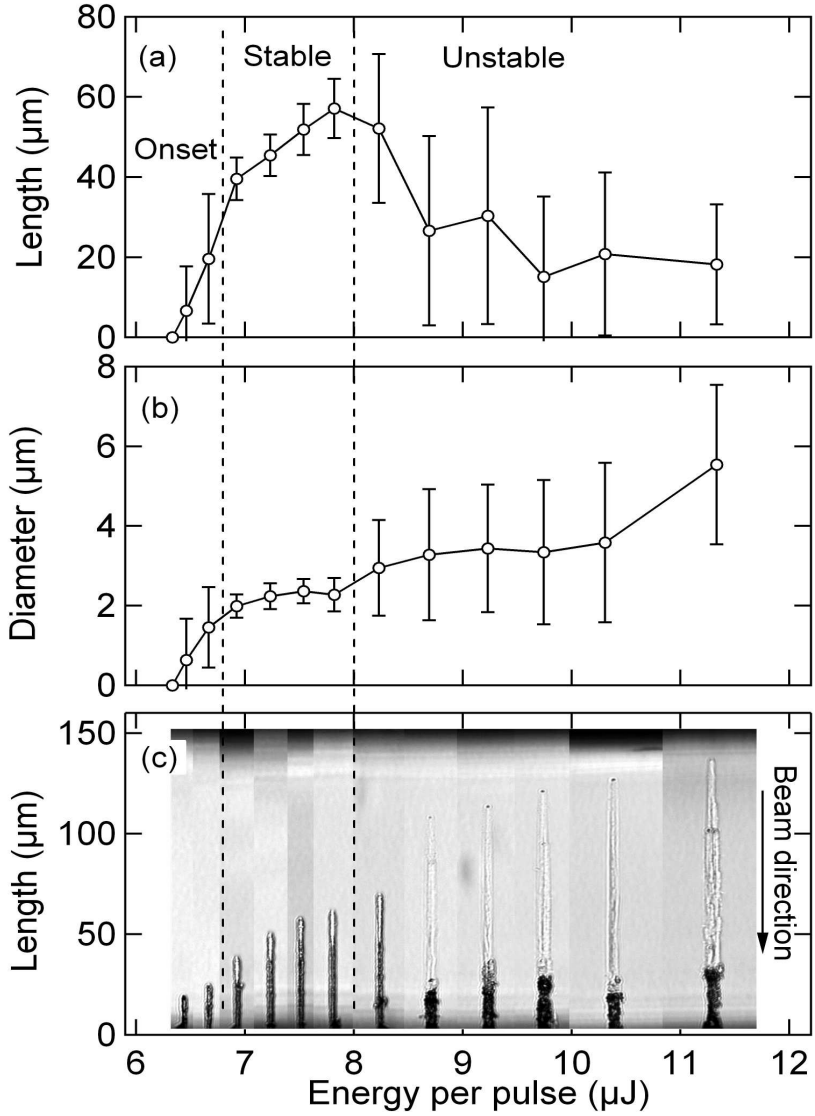

Fig. 5. Variation of (a) channel length and (b) mean channel diameter as a function of energy per pulse, using 1000 laser shots at a repetition rate of 100 Hz. Results in (c) show DIC microscopy images of typical structures observed at each energy.

In these experiments, we observed a clear threshold effect such that channel structures were only observed for energies greater than 6.2 μJ. Below this energy we observed refractive index modifications, but the properties of these index-modified structures were not examined in detail. Close to threshold (the "onset" regime defined in the figure), the individual channels within the series of 10 machined at each pulse energy displayed large variation in length and diameter, reflected in the error bars shown in the figure. However we observed a clear increase in channel length and a similar increase in channel diameter with energy and, significantly, greatly improved stability within the energy range 6.8 – 8 μJ.

Above 8 μJ, a significant qualitative change is observed: whilst the structure diameter continues to increase, the nature of the machined channel changes significantly. Specifically, the individual channels within the series of 10 that were machined at each pulse energy displayed large variation in their length and diameter. We also see from the DIC images that the machined structure exhibits significant longitudinal variability with both drilled channel

#119015 - $15.00 USD Received 23 Oct 2009; revised 30 Nov 2009; accepted 30 Nov 2009; published 4 Jan 2010
(C) 2010 OSA

(dark) and index-modified tracks (light) clearly apparent. Moreover, within the drilled channels, there is significant transverse variation. As indicated in the figure, this defines a boundary between "stable" and "unstable" channel formation.

We discuss the interpretation of these results in more detail in the following section, but at this point, it is appropriate to briefly consider the mechanism underlying the termination of the channel in the stable regime. Channel termination here can be understood physically in terms of the decrease of the intensity at the extremity of the Bessel beam below a minimum threshold for efficient ablation. This is consistent with the results in the onset and stable regimes of Fig. 5 which indeed show that the attainable channel length does scale linearly with local intensity; assuming a central lobe area of 5 μm^2 and taking into account the longitudinal variation of the Bessel beam in the sample, we estimate a threshold of ~10^{14} W/cm^2 consistent with known values for borosilicates.

Finally in this section, we comment on the surface roughness of the channels. When machining one sample, this has been quantified as typically < 400 nm, comparable to that obtained by other workers [28]. This surface nonuniformity is primarily attributed to mechanisms similar to those identified in previous studies of surface machining involving the interplay between the beam propagation and the fluid dynamics of the ablated material [14]. For the case of the Bessel beam geometry used here, the effect of the water in removing ejected material remains to be clarified and may play an important additional role.

5. Discussion and interpretation

From the practical viewpoint of using Bessel beams for microchannel fabrication, our results above are very promising. We have identified a useful working window where stable high aspect ratio microchannels can be fabricated in glass, in a highly reproducible fashion, using a setup that does not require sample translation along the channel length. Using 1000 laser shots with pulse energies in the range pulse energies in the range 7-8 μJ has been found to yield high quality taper-free channels with diameters ~2 μm and lengths in the range 40-80 μm for repetition rates in the range 1 kHz-50 Hz. With no sample translation, the "processing time" is determined only by the time to illuminate the sample with the required number of shots to drill the channel and in the case of a 1 kHz repetition rate for example, this implies that a 40 μm channel can be machined in 1 second, a significantly faster processing time than is possible with Gaussian beams where high aspect ratio drilling requires low translation speeds ~1 μm/s [14].

From a more fundamental viewpoint, our results also raise several interesting questions regarding the physics of intense femtosecond ablation processes involving Bessel beams. It is important to note that the mechanisms of structural modification we observe in our experiments are highly nonlinear. This is because the intensity levels in our experiments are above the 10^{13} W/cm^2 threshold for intensity clamping in glass where beam propagation becomes highly modified by effects such as nonlinear self-focusing, optical breakdown, filamentation and plasma formation [14,31]. In fact, our experimental results themselves provide important evidence for a nonlinear interaction mechanism, because the diameter of the machined microchannels (~2 μm) cannot be understood in terms of a purely linear ablation mechanism. This is because the calculated intensity of the Bessel beam exceeds the ablation threshold of glass out to the 4th sidelobe, and a linear mechanism would imply that all these over-threshold sidelobes would contribute to the channel formation. This would yield a channel diameter of around 20 μm, an order of magnitude greater than that observed experimentally.

Although we cannot identify the precise nonlinear mechanisms underlying the structural changes from our experiments, recent studies of femtosecond Bessel beam propagation in Kerr media allow us to suggest a scenario for channel formation in terms of filamentation. Specifically, our results are consistent with the fact that Bessel beam filamentation has been shown to establish a single and continuous plasma channel of constant density whose diameter is determined only by the central lobe (see Fig. 5 of Ref [26]). In this regard, we note that the diameter of the machined channels in our experiments is indeed comparable (within a factor

#119015 - $15.00 USD Received 23 Oct 2009; revised 30 Nov 2009; accepted 30 Nov 2009; published 4 Jan 2010
(C) 2010 OSA

of 1.3) to the diameter at half-maximum of the central lobe of the Bessel beam. Moreover, similar stable channel formation is indeed observed in the case of self-guided filament void formation and drilling in glass in Refs [9] and [23] respectively. In fact, we also remark that the channel morphology in our experiments in the unstable regime are also comparable to those seen in unstable filament propagation in Ref [25]. A filamentation mechanism is also consistent with other aspects of the results in Fig. 5. Specifically, a fluence threshold marking a transition between stable and unstable plasma channel formation has also been noted in Ref [26]. This transition arises because the formation and propagation of stable Bessel filaments requires that the intensity at the front surface is sufficiently low to avoid the immediate triggering of nonlinear effects when the beam enters the sample.

An important aspect of this interpretation is that it allows us to consider how the properties of the machined channels will be expected to vary with beam parameters. For example, based on other studies studying Bessel beam photomodification and etching [21,22], we expect the machined microchannel diameter to scale linearly with the diameter of the central lobe of the Bessel beam. It is also possible to consider important applications in extending the machined length and obtaining through-channels. At first sight, a simple approach would be to use a Bessel beam of larger depth of focus or using longitudinal translation. However, such an approach could easily lead to an increased intensity at the front surface which could trigger immediate nonlinear effects in the sample and destabilize the beam as discussed above [26]. Machining through-channels whilst avoiding front-surface induced instabilities may nonetheless be possible with a careful optimisation of beam intensity and focusing geometry but this would require further theoretical and experimental validation. An alternative approach in the first instance would be sample cleaving and/or the addition of a sacrificial layer. In a more general context, other preliminary results we have obtained indicate that a useful guideline for estimating the attainable channel length for any particular Bessel beam focusing geometry is that the distance from the point at which the Bessel beam first exceeds our estimated 10^{14} W/cm^2 threshold and the front surface exceeds approximately twice the full width at half maximum of the beam.

Of course, confirming this quantitatively will require further experiments and numerical modelling, particularly with regard to studying the interplay between optical breakdown and filamentation when using the Bessel beam focussing geometry [1].

6. Conclusions

Our results clearly show the potential of femtosecond Bessel beams for high aspect ratio microchannel machining in glass without sample translation. Our studies have determined a practical working window where amplified femtosecond lasers can be used to generate high quality structures, and taper-free channels of 2 μm diameter and with aspect ratios up to 40 have been obtained. A novel interpretation of our results in terms of a nonlinear filamentation mechanism has been proposed. We anticipate that these results will motivate further studies of the practical application of Bessel beams in materials processing and fundamental studies of the Bessel beam light-matter interaction. An important aim here has been to demonstrate the essential novelty and advantages of Bessel beam machining with the objective of motivating further research in this field. Our results suggest some immediate directions for future research to clarify a number of open questions and to study potential new applications.

Acknowledgements

We acknowledge the Région Franche-Comté, the Institut Universitaire de France and the Association des Instituts Carnot for funding. We thank S. Moëc, N. Marthouret and D. Guibert for technical assistance. M. Withford was supported by the Université de Franche-Comté invited professor scheme.